Supplementary information

Cryo-EM structures of *Candida albicans* Cdr1 reveal azole-substrate recognition and inhibitor blocking mechanisms

Ying Peng[1,4], Yan Lu[1,4], Hui Sun[1,4], Jinying Ma[2,4], Xiaomei Li[3,4], Xiaodan Han[1,4], Zhixiong Fang[1], Junming Tan[1], Yingchen Qiu[1], Tingting Qu[1], Meng Yin[1*], Zhaofeng Yan[1*]

[1]Affiliated Hospital of Hunan University/Xiangtan Central Hospital, School of Biomedical Sciences, Hunan University, Changsha 410082, China

[2]School of Life Sciences, Tsinghua University, Beijing 100084, China

[3]Shanxi Academy of Advanced Research and Innovation, Taiyuan 030032, China

[4]These authors contributed equally: Ying Peng, Yan Lu, Hui Sun, Jinying Ma, Xiaomei Li, Xiaodan Han

[*]To whom correspondence should be addressed: yinm@hnu.edu.cn (M.Y.) or zhaofengyan@hnu.edu.cn (Z.Y.)

This PDF file includes:

Supplementary Figs. 1-11

Supplementary Tables 1

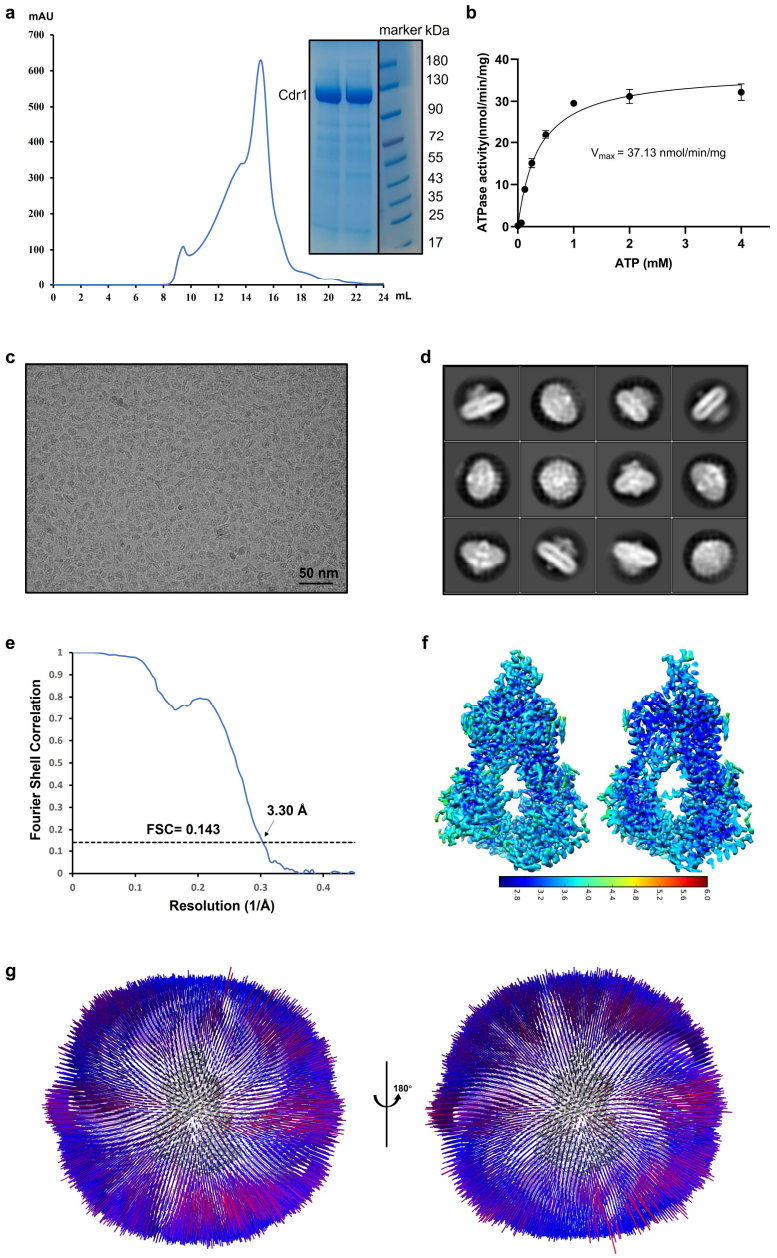

Supplementary Fig. 1 Purification and cryo-EM analysis of Cdr1^{Flu}

a, Representative size exclusion chromatogram of Cdr1 and Coomassie blue-stained SDS-PAGE gel displaying the purified peak fraction obtained from the chromatogram. **b,** ATPase activity of wild type Cdr1 (data are represented as mean ± SD; n=3; three biological repeats). **c,** Representative cryo-EM micrograph of Cdr1^{Flu}. Scale bar, 50 nm. **d,** Representative 2D classification of the Cdr1^{Flu}, with a resolution limited to 20 Å. **e,** Gold standard Fourier shell correlation (FSC) curves of the Cdr1^{Flu}. **f,** Local resolution of the density map of the Cdr1^{Flu}. **g,** Angular distribution of particle orientations in Cdr1^{Flu} samples.

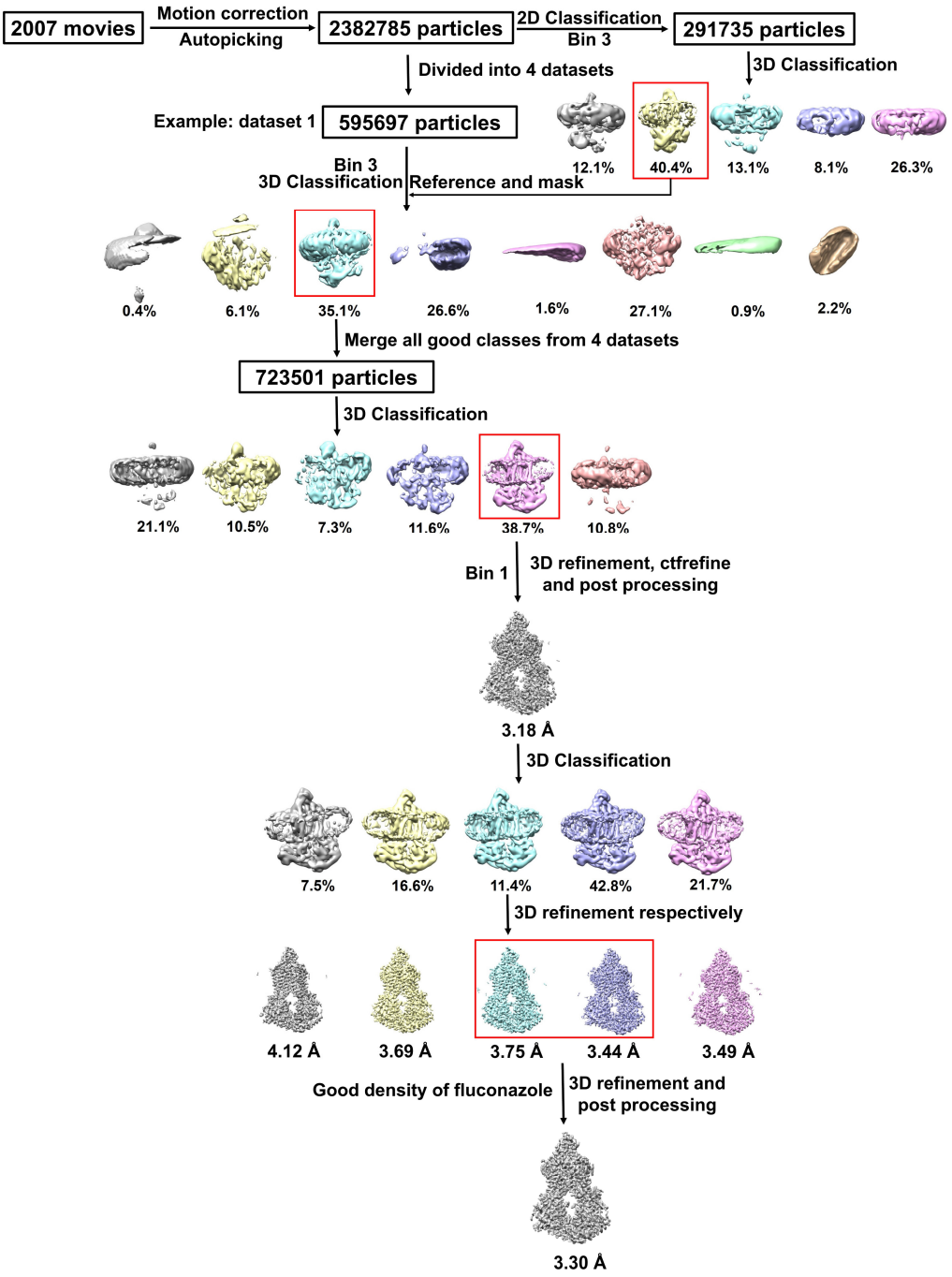

Supplementary Fig. 2 Cryo-EM data processing flowchart for Cdr1^{Flu}

The diagram illustrates the key steps in the computational analysis workflow for cryo-EM reconstruction of Cdr1 bound to fluconazole. In the final stage of 3D classification, high-quality classes featuring well-defined fluconazole density are chosen for subsequent processes, including 3D refinement and post-processing.

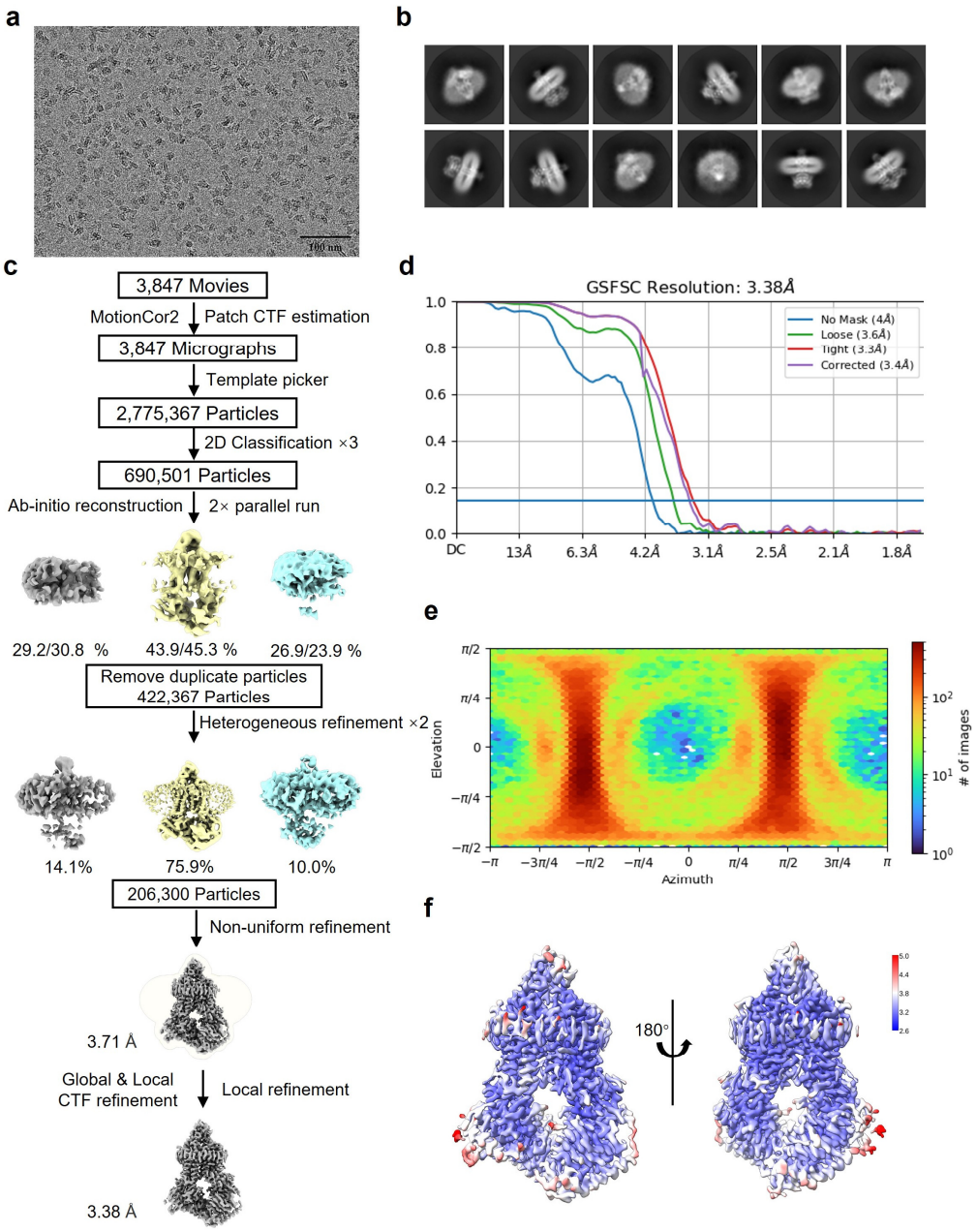

Supplementary Fig. 3 Cryo-EM image processing of Cdr1^{Apo}

a, Representative cryo-EM micrograph of Cdr1^{Apo}. Scale bar, 100 nm. **b,** Representative 2D classification of the Cdr1^{Apo}. **c,** The cryo-EM processing workflow for Cdr1^{Apo} dataset resulted in a focused refinement at 3.38 Å resolution. **d,** Gold standard FSC curves for the maps with no mask (blue), loose mask (green), tight mask (red) and corrected mask (purple). **e,** Angular distribution of the particles used for the final reconstructions. **f,** Local resolution of the density map of the Cdr1^{Apo}.

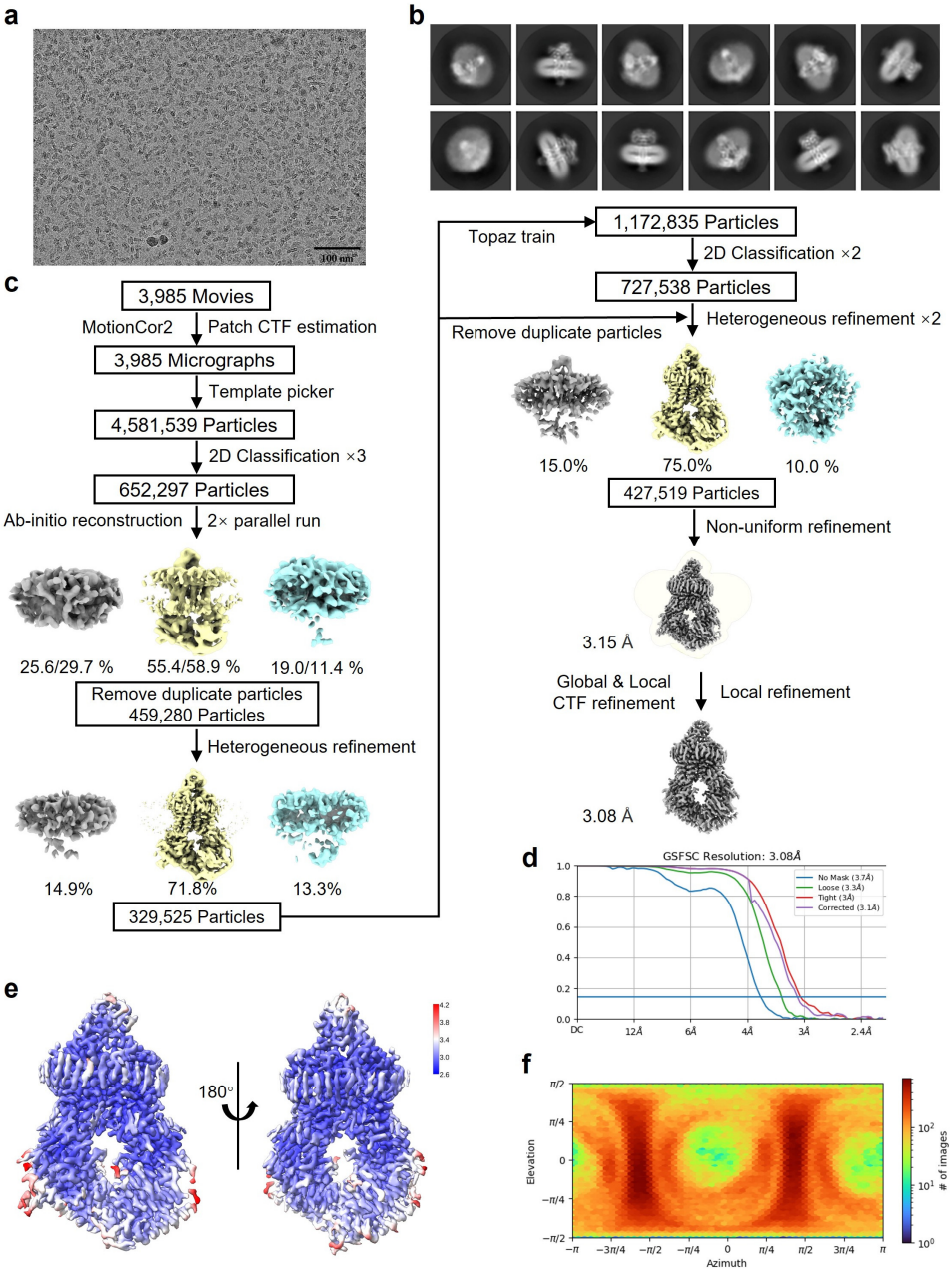

Supplementary Fig. 4 Cryo-EM image processing of Cdr1^{Mil}

a, Representative cryo-EM micrograph of Cdr1^{Mil}. Scale bar, 100 nm. **b,** Representative 2D classification of the Cdr1^{Mil}. **c,** The cryo-EM processing workflow for Cdr1^{Mil} dataset resulted in a focused refinement at 3.08 Å resolution. **d,** Gold standard FSC curves for the maps with no mask (blue), loose mask (green), tight mask (red) and corrected mask (purple). **e,** Angular distribution of the particles used for the final reconstructions. **f,** Local resolution of the density map of the Cdr1^{Mil}.

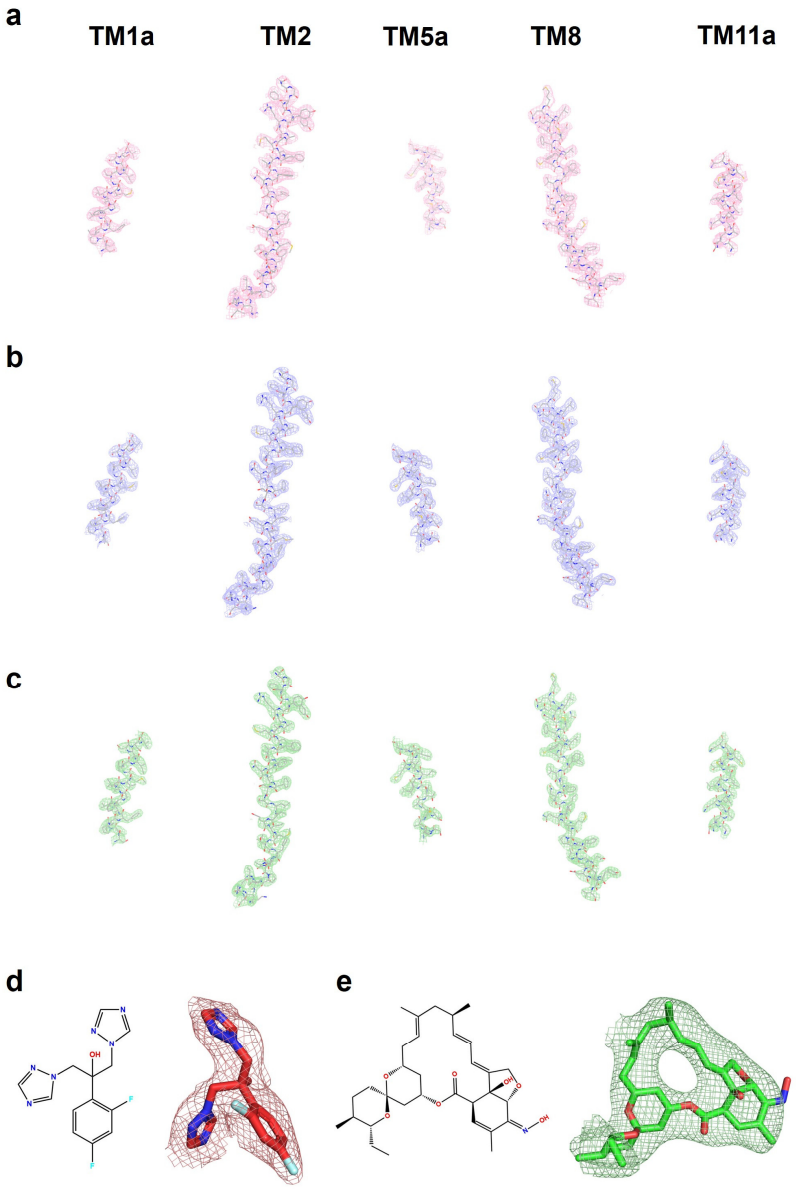

Supplementary Fig. 5 The representative cryo-EM densities at different states

a-c, Cryo-EM densities of five representative transmembrane helices (TM1a, TM2, TM5a, TM8 and TM11a) from $Cdr1^{Apo}$ (**a**), $Cdr1^{Flu}$ (**b**) and $Cdr1^{Mil}$ (**c**), respectively. **d,** Structural formula (left panel) and EM density (right panel) of fluconazole. **e,** Structural formula (left panel) and EM density (right panel) of milbemycin oxime.

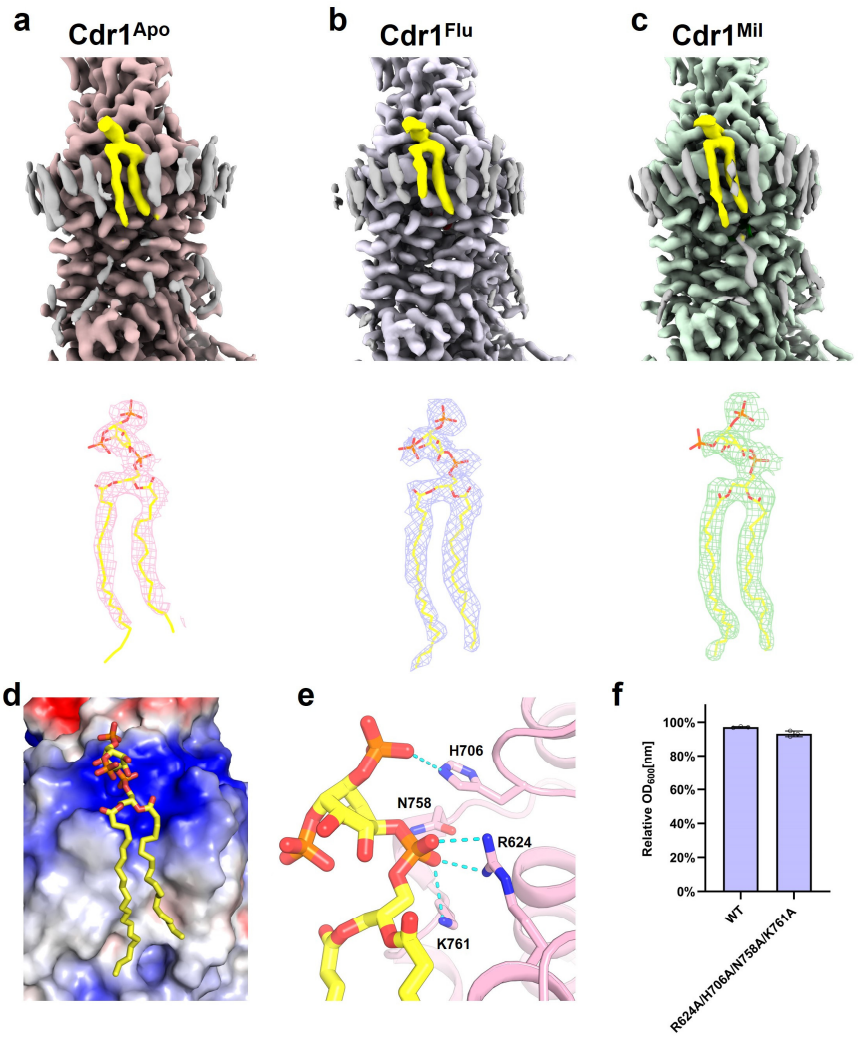

Supplementary Fig. 6 Structural analysis of PIP2 lipid bound in the exoplasmic membrane leaflet

a-c, Cryo-EM densities and locations of the PIP2 ligand (yellow) in $Cdr1^{Apo}$ (left panel), $Cdr1^{Flu}$ (middle panel) and $Cdr1^{Mil}$ (right panel). **d,** The electrostatic surface rendering for the atomic model of Cdr1. PIP2 molecular is shown as yellow sticks. **e,** Zoomed-in views of the interaction between PIP2 head group and Cdr1. Cyan dashes indicate electrostatic interaction. **f,** Relative OD_{600nm} values for wild type and mutants under a 10 µg/ml fluconazole concentration. The y-axis represents the relative OD_{600nm} values as a percentage of the control (no drug). Data are presented as mean values ± SD; n = 3 independent experiments.

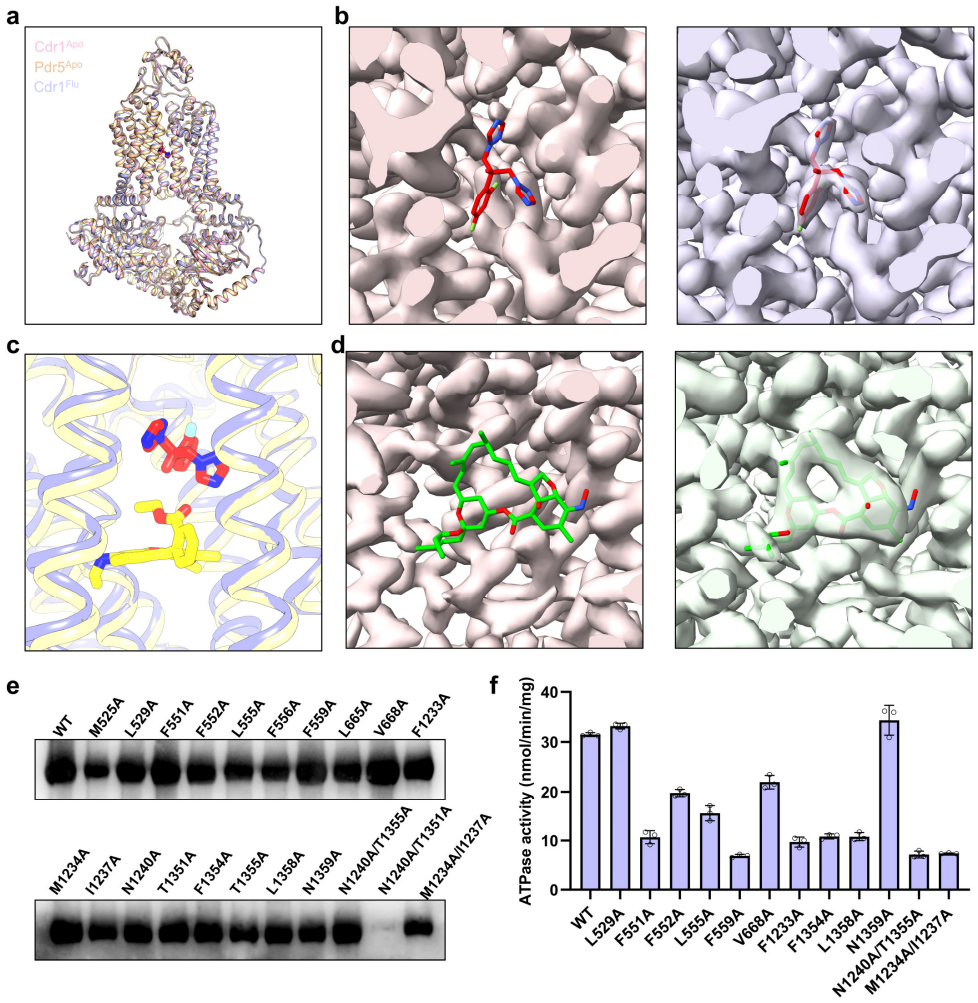

Supplementary Fig. 7 Structural analysis of fluconazole-bound Cdr1

a, Structural comparison of $Cdr1^{Flu}$ with $Cdr1^{Apo}$ and $Pdr5^{Apo}$ (PDB: 7P03). Models of $Cdr1^{Flu}$, $Cdr1^{Apo}$ and $Pdr5^{Apo}$ are colored by light-blue, pink and wheat, respectively. **b**, Cryo-EM densities of fluconazole binding region for $Cdr1^{Apo}$ (left panel) and $Cdr1^{Flu}$ (right panel). Fluconazole is well fitted in $Cdr1^{Flu}$, while $Cdr1^{Apo}$ does not have this density. **c**, Structural comparison of $Cdr1^{Flu}$ with $Pdr5^{R6G}$. Models of $Cdr1^{Flu}$ and $Pdr5^{R6G}$ are colored by light-blue and yellow, respectively. R6G is positioned beneath fluconazole. **d**, Cryo-EM densities of fluconazole binding region for $Cdr1^{Apo}$ (left panel) and $Cdr1^{Mil}$ (right panel). Milbemycin oxime is well fitted in $Cdr1^{Mil}$, while $Cdr1^{Apo}$ does not have this density. **e**, Western blotting analysis of the mutants in Fig. 2d. **f**, ATPase activity assay of the mutants that decreased fluconazole drug resistance in Fig. 2d. Cdr1 and mutants are purified in GDN detergent. Data are presented as mean values ± SD; n = 3 independent experiments.

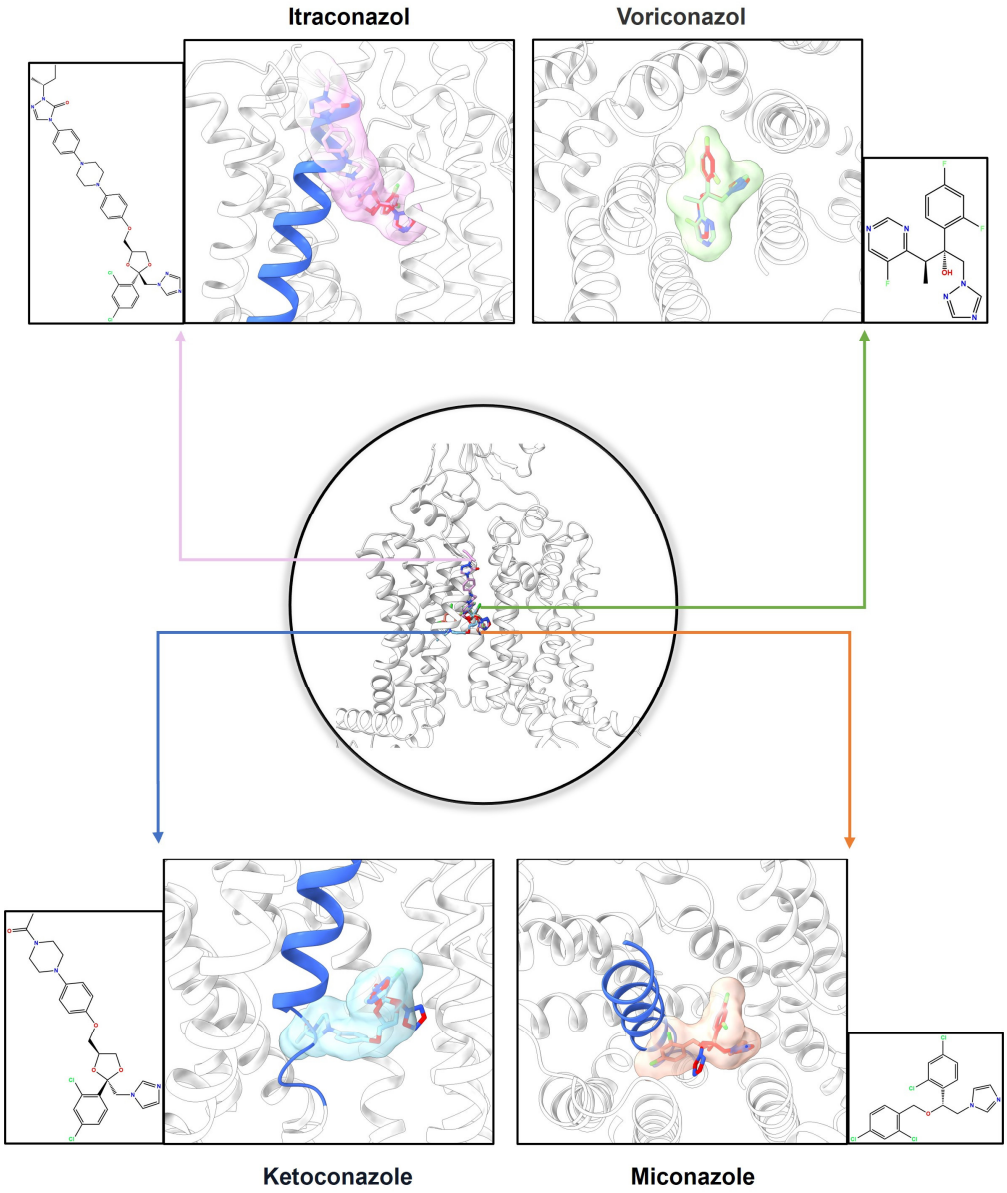

Supplementary Fig. 8 Presentative azole drugs docked in Cdr1^{Flu}

Four representative azoles were docked into the structure of Cdr1^{Flu} (central figure). Arrows of different colors point to the zoomed-in view of the docking region of each azole. The pink, green, blue, and orange arrows point to itraconazole, voriconazole, ketoconazole and miconazole, respectively. Fluconazole is shown in red. Adjacent to each docking view is the structural formula of the respective drug.

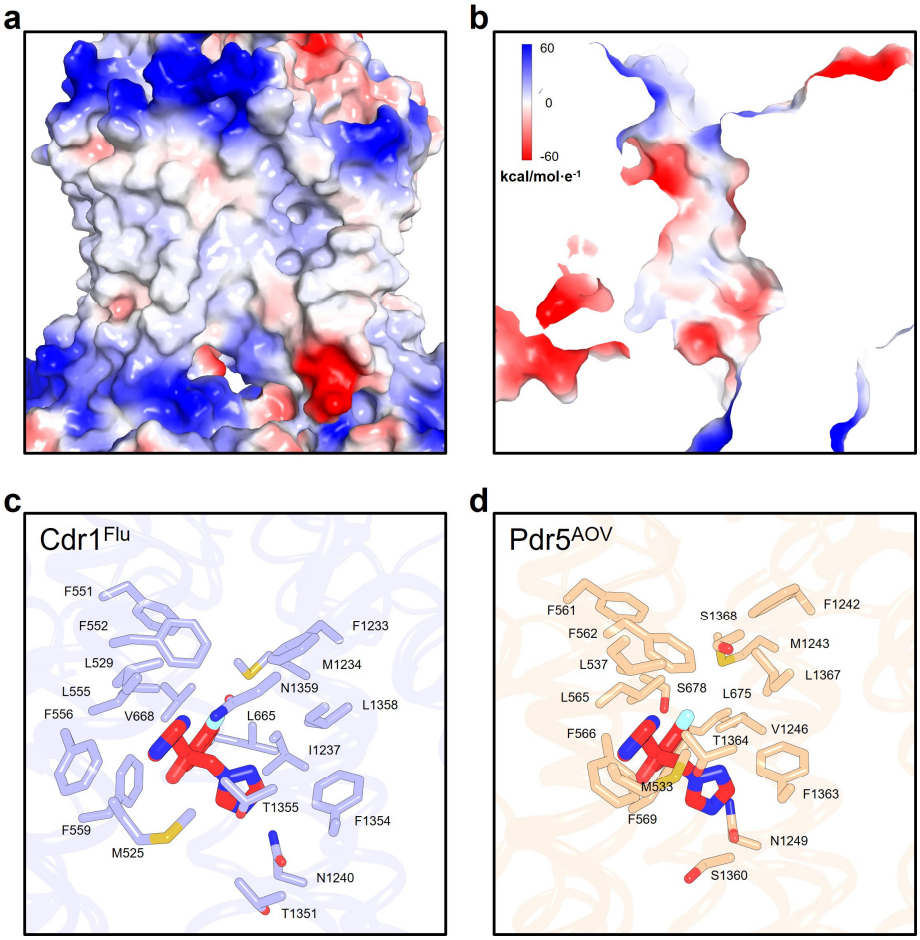

Supplementary Fig. 9 The closure of entrance channels in Pdr5^{AOV} and fluconazole binding cavities between Cdr1^{Flu} and Pdr5^{AOV}

a, b, Side (**a**) and bottom (**b**) view of electrostatic surface in Pdr5^{AOV}. Both the inner-leaflet channel (**a**) and the cytoplasmic channel (**b**) are blocked. **c, d,** The fluconazole binding cavities with Cdr1^{Flu} (**c**) or Pdr5^{AOV} (**d**). The fluconazole binding cavity in Pdr5^{AOV} ceases to exist, as some residues that originally interacted with fluconazole in the inward-facing structure move inward.

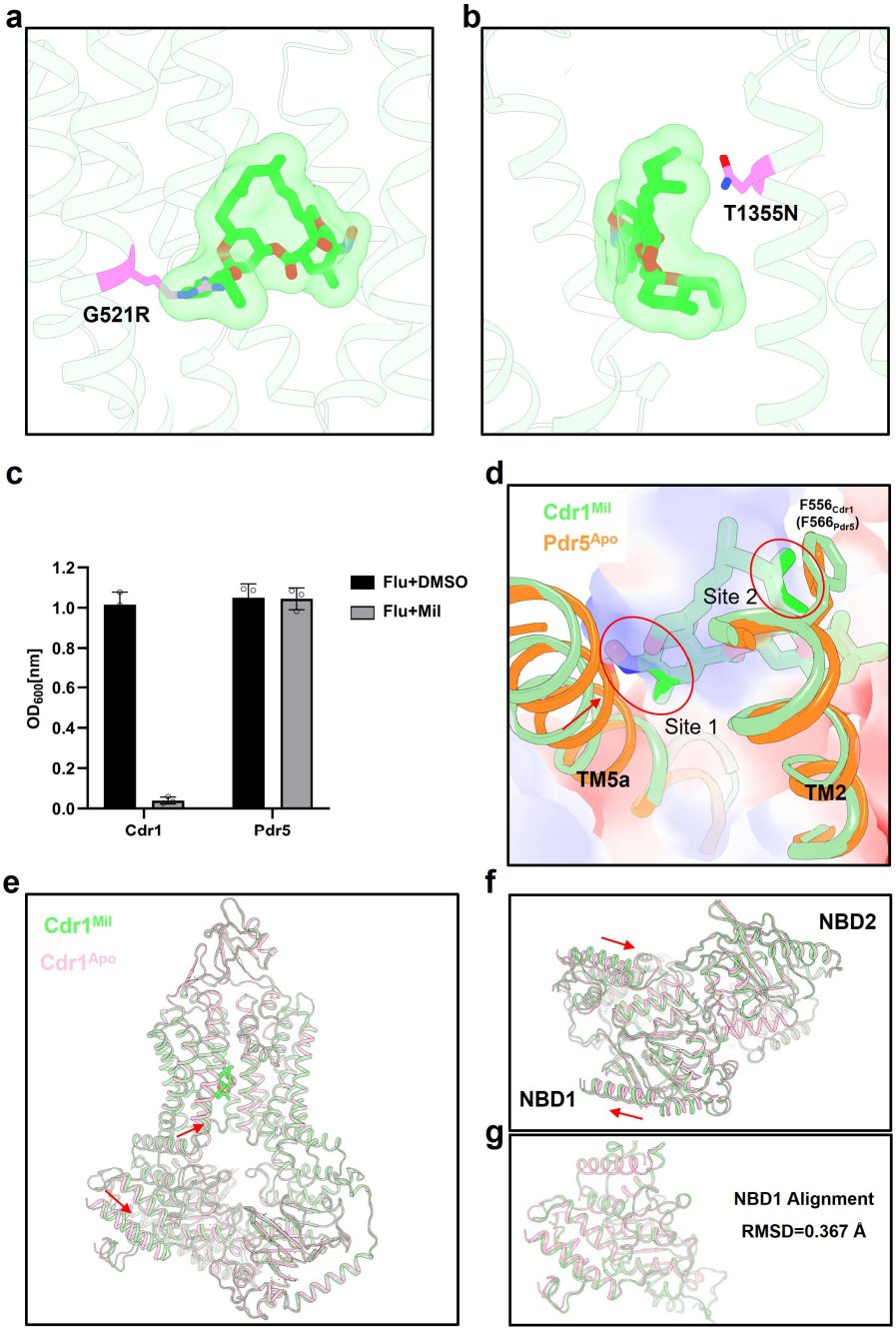

Supplementary Fig. 10 Structural analysis of milbemycin oxime-bound Cdr1

a, Spatial hindrance observed at the binding site of G521R mutation with a green-colored milbemycin oxime surface diagram in Cdr1^{Mil} (light-green). **b,** Mutation T1355N leads to a conflict between the hydrophilic nature of the side chain of asparagine and the hydrophobic nature of milbemycin oxime. **c,** Absorbance at 600nm (OD_{600}) was measured after treating overexpressed Pdr5 or Cdr1 in Pdr5-knocked-out *S. cerevisiae* with 1 μg/mL fluconazole in the presence of DMSO (black) or 0.1 μg/mL milbemycin oxime (grey). Data are presented as mean values ± SD; n = 3 independent

experiments. **d,** Structural comparison of $Cdr1^{Mil}$ (light-green) and $Pdr5^{Apo}$ (orange). TM5a in Pdr5 moves inward, resulting in steric clash with milbemycin oxime (site 1). Phe566 in Pdr5 bends inward, leading to steric clash with milbemycin oxime (site 2). **e,** Structural comparison of $Cdr1^{Mil}$ (pale-green) with $Cdr1^{Apo}$ (light-pink). Red arrows indicate the movements of the related regions. **f,** Bottom view of NBD region in $Cdr1^{Mil}$ and $Cdr1^{Apo}$ reveals evident movements in NBD1. **g,** Structural alignment of individual NBD1 domains from $Cdr1^{Mil}$ and $Cdr1^{Apo}$ reveals a low RMSD value of 0.367 Å, indicating a rigid movement between this region.

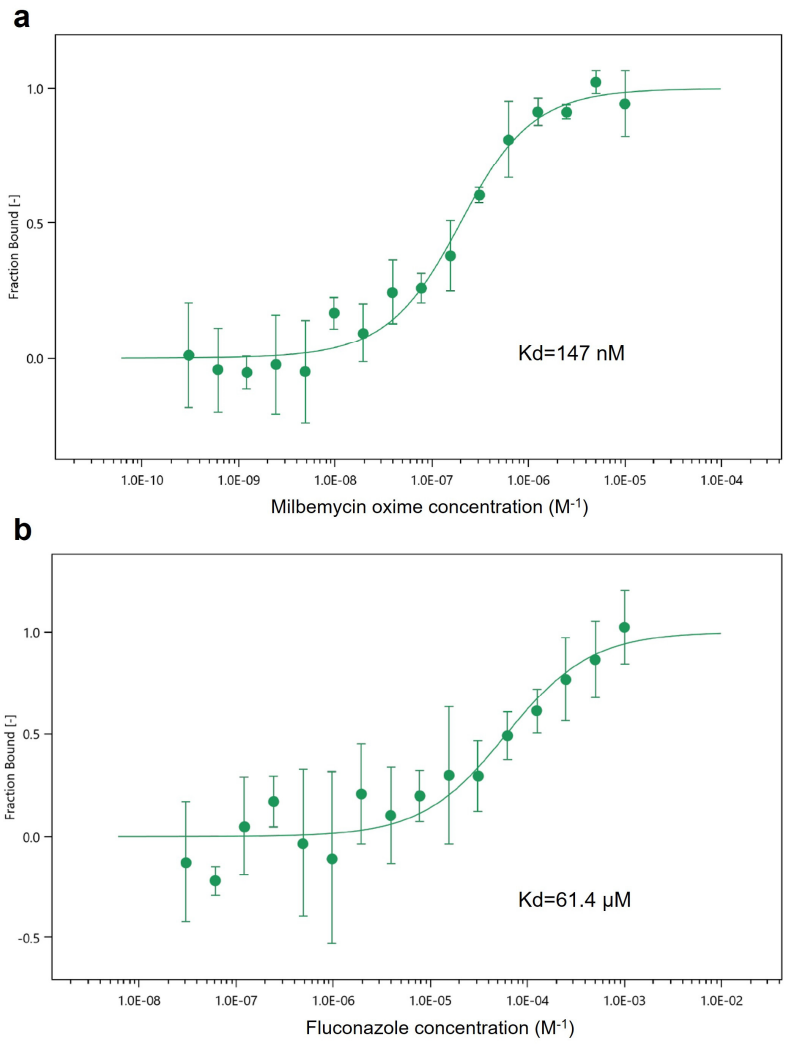

Supplementary Fig. 11 The binding affinities of Cdr1 with milbemycin oxime and fluconazole

a-b, The binding affinities of Cdr1 with milbemycin oxime (**a**) and fluconazole (**b**) were measured using MST assays. The dissociation constants (Kd) were determined to be 147 nM for milbemycin oxime and 61.4 µM for fluconazole. Each assay was performed in triplicate. The figures were generated using MO. Affinity Analysis v.2.3 software. Data are presented as mean values ± SD; n = 3 independent experiments.

Supplementary Table 1. Cryo-EM data collection, refinement and validation statistics.

	$Cdr1^{Apo}$	$Cdr1^{Flu}$	$Cdr1^{Mil}$
Data collection and processing			
Magnification	105000	105000	81000
Voltage (kV)	300	300	300
Electron exposure ($e^-/Å^2$)	50	50	55
Defocus range (μm)	-1.5 to -2.1	-1.5 to -2.1	-1.5 to -2.1
Pixel size (Å)	0.837	0.837	1.088
Symmetry imposed	C1	C1	C1
Final particle images (no.)	206,300	201,731	427,519
Map resolution (Å)	3.38	3.30	3.08
FSC threshold	0.143	0.143	0.143
Map sharpening *B* factor ($Å^2$)	-148.4	-127.7	-153.1
Refinement			
R.m.s deviations			
Bond lengths (Å)	0.003	0.003	0.003
Bond angles (°)	0.530	0.436	0.468
Validation			
Molprobity score	1.42	1.40	1.46
Clashscore	6.03	4.42	4.66
Poor rotamers (%)	0.18	0.44	0.26
Ramachandran plot			
Favored (%)	97.58	96.98	96.52
Allowed (%)	2.42	3.02	3.48
Disallowed (%)	0.00	0.00	0.00